# *Courbure discrète : théorie et applications*

Rencontre organisée par :
Laurent Najman and Pascal Romon

18-22 novembre 2013

Yonathan Aflalo, Anastasia Dubrovina, Ron Kimmel, and Aaron Wetzler

**Curvature in image and shape processing**

Vol. 3, n° 1 (2013), p. 131-139.

<http://acirm.cedram.org/item?id=ACIRM_2013__3_1_131_0>

Centre international de rencontres mathématiques
U.M.S. 822 C.N.R.S./S.M.F.
Luminy (Marseille) France

Actes des rencontres du C.I.R.M.
Vol. **3** n° 1 (2013) 131-139

# Curvature in image and shape processing

Yonathan Aflalo, Anastasia Dubrovina, Ron Kimmel, and Aaron Wetzler

**Abstract**

The laplacian operator applied to the coordinates of a manifold provides the mean curvature vector. Manipulating the metric of the manifold or interpreting its coordinates in various ways provide useful tools for shape and image processing and representation. We will review some of these tools focusing on scale invariant geometry, curvature flow with respect to an embedding of the image manifold in a high dimensional space, and object segmentation by active contours defined via the shape laplacian operator. Such generalizations of the curvature vector and its numerical approximation as part of an image flow or triangulated shape representation, demonstrate the omnipresence of this operator and its usefulness in imaging sciences.

## 1. Introduction

The total variation [25] image selective smoothing filter, the Beltrami flow for color image processing [28, 24, 32] and its close relative the bilateral filter [30, 27], the affine invariant flow for images [10, 3] are all reincarnations of considering the heat flow defined by second derivative of a manifold with respect to its associated arc length. Strictly speaking, from a differential geometry point of view, the laplacian operator does not always defines the curvature, especially when non-trivial invariants are involved. Yet, this geometric structure has been found to be very practical in shape and image processing.

At the other end, the laplacian operator can be decomposed into its eigenfunctions and eigenvalues, which provide a generalization of the classical Fourier decomposition to non-trivial manifolds and non-regular parameterizations. Such a bases were introduced into the shape analysis arena in the last decade, see for example [18, 19]. The resulting eigenfunctions are sometimes referred to as the natural basis, as it can be shown to be the optimal basis for representing smooth functions on the given manifold [1]. Here, we will review several applications of the laplace Beltrami operator (LBO) in which we allow ourself to define the metric according to the problem at hand. The resulting heat operator or natural basis by decomposition of the LBO would allow us to process images and shapes with the same framework. In a sense, this paper is more a pedagogical overview rather than a specific contribution. To that end, let us start with a simple example of how a new definition of a pseudo-metric could lead to a scale invariant geometry for shapes.

## 2. On geometries and natural eigenbases

Sochen suggested to plugged invariant metrics into the definition of the laplacian in order to extract corresponding invariant eigenfunctions and eigenvalues for image processing [29]. Later on, Raviv et al. [23] used this observation to construct an equi-affine invariant pseudo metric for surfaces, while two of us and Raviv [2] introduced a scale invariant geometry and produced a corresponding natural basis for shapes. To exemplify the properties of such a methodology,

Text presented during the meeting "Discrete curvature: Theory and applications" organized by Laurent Najman and Pascal Romon. 18-22 novembre 2013, C.I.R.M. (Luminy).
2000 *Mathematics Subject Classification.* 00X99.
*Key words.* Image denoising, scale invariant, active contours, segmentation.
This research was supported by European Community FP7-ERC program, grant agreement no. 267414.

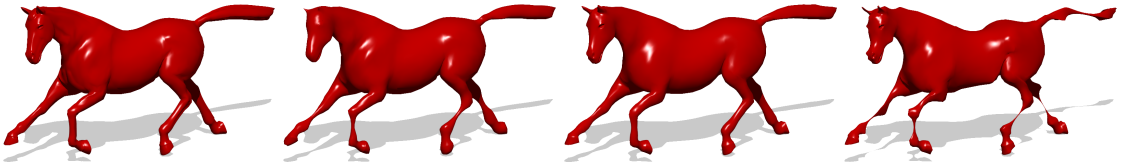

Figure 2.1: From left to right: A horse, Coordinates projected to the first 300 eigenfunctions (regular metric), Coordinates projected to the first 300 eigenfunctions (mixed metric). Coordinates projected to the first 300 eigenfunctions (scale invariant metric).

here, we start from an arc length construction followed by a metric definition and decompose the corresponding LBO into a natural basis structure that we then apply to shape representation.

Let $S(u,v):\Omega\subset\mathbb{R}^2\to\mathbb{R}^3$ be a parametrized surface embedded in $\mathbb{R}^3$. Next, let $C(p):[0,1]\to S$ be a parametrized curve in $S$, for which we can define the total arc length to be

$$\text{Length}(C)=\int_0^1|C_p|dp=\int_0^1|S_u u_p+S_v v_p|dp=\int_0^1\sqrt{|S_u|^2u_p^2+2\langle S_u,S_v\rangle u_p v_p+|S_v|^2v_p^2}dp. \tag{2.1}$$

Denoting the metric coefficients $g_{ij}=\langle S_i,S_j\rangle$ where $i,j\in\{u,v\}$ we readily have the arc length on the surface defined by $ds^2=\sum_{i=\{u,v\}}\sum_{j=\{u,v\}}g_{ij}didj$. Using Einstein summation convention, the Laplace-Beltrami operator is given by

$$\Delta_g\equiv\frac{1}{\sqrt{g}}\partial_i\sqrt{g}g^{ij}\partial_j, \tag{2.2}$$

where $g$ is the determinant of the metric $(g)$, the inverse metric coefficients are $g^{ij}=\left((g)^{-1}\right)_{i,j}$, and $\partial_i$ is the derivative with respect to the $i^{\text{th}}$ coordinate, $u$ or $v$ in our case.

The operator $\Delta_g$ admits a spectral decomposition with an orthogonal eigenbasis $\{\phi_k\}$ and a set of corresponding eigenvalues $\{\lambda_k\}$ defined by

$$\Delta_g\phi_k=\lambda_k\phi_k,\quad \langle\phi_k,\phi_k\rangle_g=1,\ \text{ and }\ \langle\phi_k,\phi_l\rangle_g=0,\ \forall k\neq l. \tag{2.3}$$

The choice of an invariant metric is obviously important in the context of shape representation, alignment, and matching. To that end, various distances have been proposed, such as Euclidean [12, 5], geodesic [16, 21, 17, 20], diffusion [4, 14, 9], and affine invariant versions thereof [23]. A scale invariant geometry which is also intrinsic (embedding invariant) was introduced in [2] by which the regular metric is multiplied by the Gaussian curvature,

$$\tilde{g}_{ij}=|K|g_{ij}=|K|\langle S_i,S_j\rangle. \tag{2.4}$$

Fig. 2.1 depicts the effect of representing a shape's coordinates projected to the natural basis with a regular metric compared to the scale invariant one. The idea is to use just the first few eigenfunctions as an approximation for smooth functions on the manifold treating the coordinates as such. While the regular natural basis captures the global structure of the surface, as expected, the scale invariant basis concentrates at the fine features with effective curvature. Fig. 2.2 presents an application of the generalized multidimensional scaling algorithm [8] using the scale invariant diffusion distance to extract the correspondence between an armadillo and its deformed version In these examples the LBO produced a proper basis to represent and match shapes subject to a specific yet general enough deformations. Next we will show how the LBO can be applied as a non-local heat operator acting as a powerful selective smoothing filter in image denoising.

## 3. Beltrami selective smoothing in patch space

An image $I(x,y)$ can be thought of as a two dimensional surface embedded in the hybrid spatial-intensity space. The laplacian operator of the image manifold can then be used to define a heat flow applied as a filter to the image as initial condition

$$I_t=\Delta_g I,\quad \text{given }\ I(x,y;0)=I_0. \tag{3.1}$$

The time $t$ such a flow acts on the image should somehow reflect the amount of noise in the image, while the metric $g$ could be the image metric. The hope is that such a curvature flow

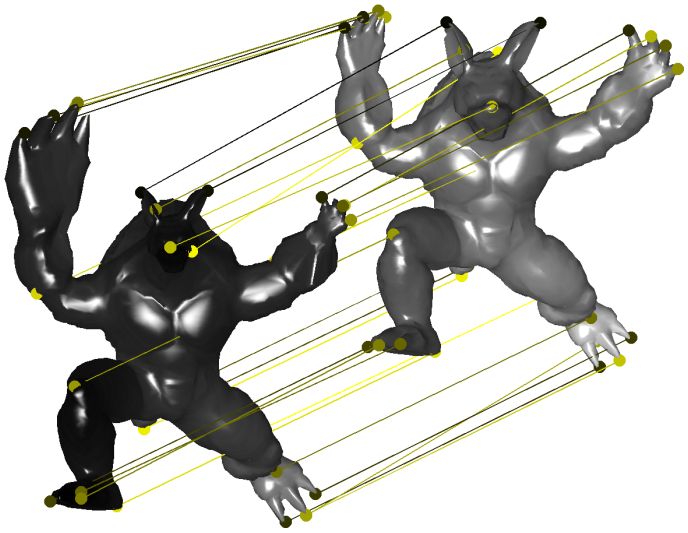

Figure 2.2: Matching an Armadillo and its locally scaled version using GMDS with the scale invariant metric.

would selectively smooth the image in a desirable fashion. The Beltrami-flow [28] considers a color image as a mapping between the spatial domain to the spatial-spectral domain, that is $I(x,y) : \Omega \in \mathbb{R}^2 \to \mathbb{R}^5$. The coordinates in the embedding space are $x, y, R, G, B$ where the last three coordinates stand for the color space Red, Green, and Blue, respectively. The resulting heat equation $I_t = \Delta_g I$ defined by the metric $g$ is usually derived from an infinitesimal arc length such as $ds^2 = dx^2 + dy^2 + dR^2 + dG^2 + dB^2$.

One non-differential version of the Beltrami flow is known as the bilateral filter [31], in which the short time kernel of the Beltrami flow is replaced by $\delta(s,s')^2 = \delta(x,x')^2 + \delta(y,y')^2 + \delta(R,R')^2 + \delta(G,G')^2 + \delta(B,B')^2$, where $\delta(x,x')^2 = (x-x')^2$. Roughly speaking, instead of convolving with the continuous version $e^{-(\int_s^{s'} ds)^2}$ in the Beltrami flow, the bilateral filter applies $e^{-\delta(s,s')^2}$ as a selective smoothing kernel.

Roussos and Maragos [24] followed by [32] extended the Beltrami flow approach by treating images as two dimensional manifolds embedded in *patch-space*. The superior denoising results of these methods coupled with their computational efficiency indicated that the Beltrami flow in its general form is well suited for dealing with image denoising. An example of the selective smoothing property of the Beltrami flow in patch space is depicted by Fig. 3.1.

In order to simplify the construction of such filters consider a height profile $I$ to be a two dimensional Riemannian manifold embedded in a higher dimensional space. We define the patch-space mapping $P : \Omega \in \mathbb{R}^2 \to S \in \mathbb{R}^{n(2w+1)^2+2}$ such that

$$P(x,y) = \left(x, y, \left\{I^k_{i,j}\right\}\right), \tag{3.2}$$

for $i,j = -w,..,w, \quad k = 1,..,n$ ,where $w \in \mathbb{N}$ is the window size, $n$ is the number of channels we use, and $\{I^k_{i,j}\}$ is the compact form for $\left\{I^k\left(x+i, y+j\right)\right\}$. For the case of a single height profile or a gray level image $n = 1$, where if we were provided with a set of registered scans of a particular surface or a color image, $n$ could represent the number of scans or colors. The manifold $P$ is equipped with a metric $g$, that defines an arc length

$$ds^2 = (dx\ dy)\,(g)\begin{pmatrix} dx \\ dy \end{pmatrix}. \tag{3.3}$$

Specifically, the patch-space metric is given by application of chain rule $dI^k_{i,j} = \partial_x I^k_{i,j} dx + \partial_y I^k_{i,j} dy$ from which it follows that

$$(g) = \begin{pmatrix} 1 + \sum_{i,j,k} (\partial_x I^k_{i,j})^2 & \sum_{i,j,k} \partial_x I^k_{i,j} \partial_y I^k_{i,j} \\ \sum_{i,j,k} \partial_x I^k_{i,j} \partial_y I^k_{i,j} & 1 + \sum_{i,j,k} (\partial_y I^k_{i,j})^2 \end{pmatrix}. \tag{3.4}$$

Figure 3.1: Examples of Beltrami patch denoising for images. From top to bottom, left to right a) Noisy Barbara, $\sigma = 21$ b) Denoised image, PSNR = 28.4dB c) Noisy Peppers, $\sigma = 30$ d) Denoised image, PSNR = 28.0dB

This metric allows us to measure distances and areas on the manifold $P$ using the coordinates of $\Omega$. For example, the area of the embedding into a Euclidean space is given by

$$\iint \sqrt{\det(g)}dxdy. \tag{3.5}$$

We minimize Eq. (3.5) using variational calculus and arrive at the EL equation

$$\Delta_g I^k_{i,j} = \frac{1}{\sqrt{g}}\mathrm{div}\big(\sqrt{g}(g)^{-1}\nabla I^k_{i,j}\big) = 0. \tag{3.6}$$

The resulting operator is indeed the LBO, and the image can thus be filtered by the corresponding Beltrami flow in patch space

$$I_t = \Delta_g I. \tag{3.7}$$

Point clouds and meshes are often assumed to have noise which is Gaussian and appears as an offset along the normal direction of the surface. For that kind of noise the mean curvature flow could produce a reasonable filter. Yet, the noise model for range scanners exhibits offsets in the direction of the camera's focal point. Moreover, the noise is seldom Gaussian and usually includes regions with missing data. This presents a challenge to state of the art denoising algorithms that are usually tuned for optimal removal of additive white noise. One of the popular denoising methods is the BM3D [15] to which we compare the Beltrami patch denoising for a depth profile obtained from a real scanner, as seen in Fig. 3.2. It appears that the method is able to selectively smooth the data while preserving the important features. The usage of the LBO as a non-local denoising filter is not our final stop. Next, we show how it can be used to formulate the geodesic active contour model in a new and novel formulation.

## 4. An LBO perspective on geodesic active contours

This section links between the Laplace-Beltrami operator, the associated heat flow towards a minimal surface, and the Geodesic Active Contours (GAC) model for image segmentation [11]. Related efforts include Bresson's *et al.* [7], expressing the GAC flow as a minimizer of the *weighted Polyakov action*, and the formulation by Bogdanova *et al.* [6]. Sochen *et al.* [26] reviewed the

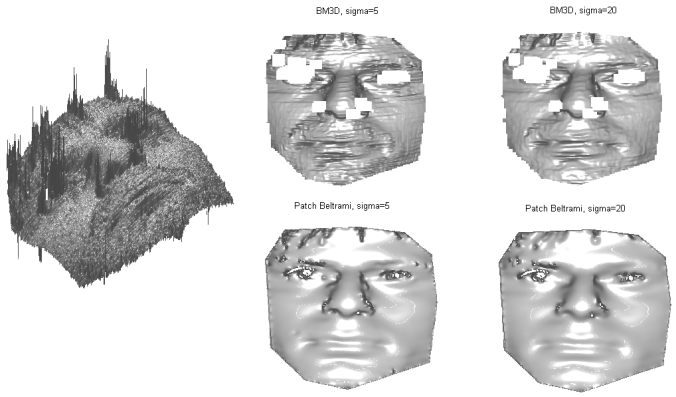


Figure 3.2: Far left: Original noisy scan. Top row: BM3D results for $\sigma = 5$ and $\sigma = 20$. Bottom row: Beltrami patch denoising for $\sigma = 5$ and $\sigma = 20$.

image filtering problem, exploring the relation between the PDE geometric approaches, derived by minimizing the Polyakov action with an appropriate metric, and non-linear robust-statistics filters. We start by reviewing the geodesic active contour model and the evolution towards generalized minimal surface.

4.1. **Geodesic active contours.** The geodesic active contour is a geometric-variational model for boundary detection, integration, and object segmentation in images. In [13] it was shown that contours extracted by this model are minimal geodesics in a Riemannian space whose metric is defined by the image intensity $I(x, y)$. We search for curves $C(p) : [0, 1] \to \mathbb{R}^2$ that minimize the following weighted Euclidean arc length

$$\int f\left(|\nabla I\left(C(p)\right)|\right)|C'(p)|\,dp = \int f\left(|\nabla I\left(C(s)\right)|\right)ds, \tag{4.1}$$

in a Riemannian space equipped with the metric tensor $f\left(|\nabla I\left(C\right)|\right)\delta_{ij}$. The function $f(x, y)$ is an edge indicator function, for example $f(x, y) = (1 + |\nabla I|)^{-1}$, designed to stop the active contour when it arrives at the object's boundary. The Euclidean arc length is denoted by $s$, where $ds = |C'(p)|dp$. Caselles *et al.* used a gradient-descent method to minimize the weighted arc length (4.1), to obtain the following curve evolution equation

$$\frac{\partial C(t)}{\partial t} = \left(f\kappa - \nabla f \cdot \vec{N}\right)\vec{N}, \tag{4.2}$$

where $\kappa\vec{N} = C_{ss}$, with $\kappa$ is the curvature of $C$, and $\vec{N}$ its unit inward pointing normal.

The level set formulation [22] of the geodesic problem (4.2) is given by

$$\frac{\partial u}{\partial t} = |\nabla u|\,\mathrm{div}\left(f\frac{\nabla u}{|\nabla u|}\right) = f\,|\nabla u|\,\mathrm{div}\left(\frac{\nabla u}{|\nabla u|}\right) + \nabla f \cdot \nabla u, \tag{4.3}$$

where $u(x, y; t)$ is an implicit representation, often referred to as a level set function, of the evolving contour $C(p; t)$. That is, $C(t) = \{(x, y) : u(x, y; t) = 0\}$, and $\kappa = \mathrm{div}\left(\frac{\nabla u}{|\nabla u|}\right)$ is the curvature of the level sets of the function $u$. The level set evolution formulation in Eq. (4.3) can be interpreted as a generalized minimal surface flow. To that end, we apply the methodology provided by Sochen *et al.* in [28] as described next.

4.2. **Generalized minimal surface flow.** Let us treat the level set function $u(x, y)$ as a two-dimensional surface embedded in a 3-dimensional space. It can be defined by the map $\mathbf{X} : \Omega \in \mathbb{R}^2 \to M \in \mathbb{R}^3$, where $\Omega$ denotes a 2D coordinates manifold $(\sigma_1, \sigma_2)$, and $M$ is the embedding space. Explicitly, $\mathbf{X}$ is written as $\mathbf{X} = \big(X^1(\sigma^1, \sigma^2), X^2(\sigma^1, \sigma^2), X^3(\sigma^1, \sigma^2)\big)$. Both manifolds $\Omega$ and $M$ are equipped with metric tensors, $g_{\mu\nu}(\sigma^1, \sigma^2)$ and $h_{ij}(x^1, x^2, x^3)$, respectively. The map $\mathbf{X}$ and the metric $h_{ij}$ can be used to construct the metric on $\Omega$

$$g_{\mu\nu}(\sigma^1, \sigma^2) = h_{ij}(\mathbf{X})\partial_\mu X^i \partial_\nu X^j, \tag{4.4}$$

where we used Einstein's summation convention. Next, the following functional can be associated with the map $\mathbf{X} : \Omega \to M$,

$$S\left[X^i, g_{\mu\nu}, h_{ij}\right] = \int d^m\sigma \sqrt{g} g^{\mu\nu} \partial_\mu X^i \partial_\nu X^j h_{ij}(\mathbf{X}), \tag{4.5}$$

where $g^{\mu\nu}$ is the inverse of the metric $g_{\mu\nu}$ (that is $g^{\mu\gamma} g_{\gamma\nu} = \delta_{\mu\nu}$), and $g$ is the determinant of $(g_{\mu\nu})$. This functional is known as Polyakov action, and it can be viewed as a generalized area measure. In fact, we already used a particular instance of the Polyakov action in Section 3, Eq. (3.5).

The minimal map (embedding) $\mathbf{X}$ can be obtained by steepest-descent. The gradient of the Polyakov action with respect to the embedding is

$$-\frac{1}{2\sqrt{g}} h^{il} \frac{\delta S}{\delta X^l} = \frac{1}{\sqrt{g}} \partial_\mu \left(\sqrt{g} g^{\mu\nu} \partial_\nu X^i\right) + \Gamma^i_{jk} \partial_\mu X^j \partial_\nu X^k g^{\mu\nu}. \tag{4.6}$$

In order to find the minimal embedding, Sochen *et al.* [28] used the gradient descent flow

$$X^i_t = -\frac{1}{2\sqrt{g}} h^{il} \frac{\delta S}{\delta X^l} = \Delta_g X^i + \Gamma^i_{jk} \partial_\mu X^j \partial_\nu X^k g^{\mu\nu}. \tag{4.7}$$

Note, that the gradient (4.6) is obtained by multiplying the Euler-Lagrange equations of (4.5) by a strictly positive function and a positive definite matrix, that will be referred to as a *pre-factor*. It could also be viewed as an indication of the metric of the variational inner product by which the gradient descent is defined. It provides a geometric parameterization-invariant flow with the same minimum. The pre-factor required to produce the GAC flow is different, stemming from the different geometry of the problem. The second term at the right hand side of Eq. (4.6) involves the Levi-Civita connection coefficients $\Gamma^i_{jk}$, that depict the geometry of the embedding space. When $M = \mathbb{R}^3$ with Euclidean metric, $h_{ij} = \delta_{ij}$, the second term vanishes, and the flow becomes $X_t = \Delta_g X$, as seen in the previous sections.

4.3. **Back to GAC: level set formulation as a flow toward minimal surface.** Next, we show that the level set formulation for geodesic active contour evolution in Eq. (4.3) is obtained by minimizing a generalized area measure. First, let us select $\mathbf{X}$ that maps the plane $(\sigma^1 = x, \sigma^2 = y)$ to a 3D Euclidean space, such that

$$\mathbf{X} = (x, y, u(x, y)). \tag{4.8}$$

The functional we would like to study is

$$S = \iint f(|\nabla I(x, y)|) \sqrt{1 + |\nabla u|^2} dx dy, \tag{4.9}$$

This is Polyakov action obtained by choosing the following metric tensors for the parameter and the embedding spaces $\Omega$ and $M$, respectively

$$\begin{aligned} g_{\mu\nu} &= f(\sigma^2, \sigma^2) \left(\partial_\mu X \cdot \partial_\nu X\right), \\ h_{ij} &= f(x^1, x^2) \delta_{ij}. \end{aligned} \tag{4.10}$$

Since $g_{\mu\nu}$ and $h_{ij}$ are legitimate metric tensors, and as $(\sigma^2, \sigma^2) = (x, y)$ and $(x^1, x^2, x^3) = (x, y, z)$, Eq. (4.4) holds.

The metric tensor $g_{\mu\nu}$, written in a matrix form becomes

$$(g_{\mu\nu}) = f \begin{pmatrix} 1 + u_x^2 & u_x u_y \\ u_x u_y & 1 + u_y^2 \end{pmatrix}. \tag{4.11}$$

The metric determinant is $g = \det(g_{\mu\nu}) = f^2 \left(1 + |\nabla u|^2\right)$ and the inverse of the metric is

$$(g_{\mu\nu})^{-1} = (g^{\mu\nu}) = \frac{f}{g} \begin{pmatrix} 1 + u_y^2 & -u_x u_y \\ -u_x u_y & 1 + u_x^2 \end{pmatrix}. \tag{4.12}$$

Next, we use Eq. (4.6) to obtain the gradient-descent flow for the level set function component of $\mathbf{X}$, namely $X^3 = u(x, y)$,

$$u_t = X^3_t = \frac{1}{\sqrt{g}} \partial_\mu \left(\sqrt{g} g^{\mu\nu} \partial_\nu u\right) + \Gamma^3_{jk} \partial_\mu X^j \partial_\nu X^k g^{\mu\nu}. \tag{4.13}$$

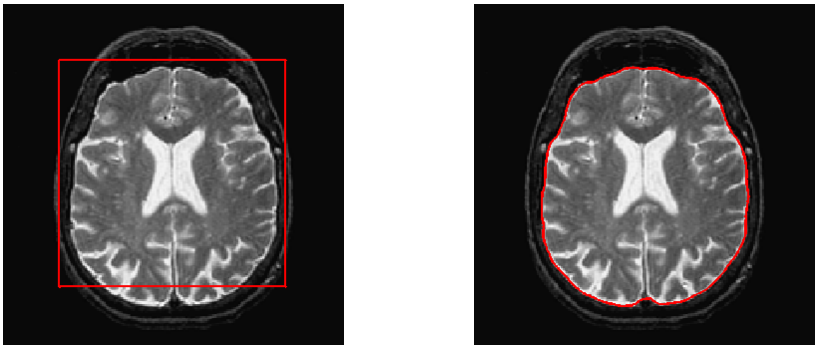

Figure 4.1: Image segmentation using Geodesic Active Contours: the initial contour (left) and the final segmentation (right).

Substituting the expressions for $\sqrt{g}$ and $g^{\mu\nu}$ into the first term of the right-hand side of the flow in Eq. (4.13) produces

$$\frac{1}{\sqrt{g}}\partial_\mu\left(\sqrt{g}g^{\mu\nu}\partial_\nu u\right) = \frac{1}{f\sqrt{1+|\nabla u|^2}}\mathrm{div}\left(\frac{\nabla u}{\sqrt{1+|\nabla u|^2}}\right). \tag{4.14}$$

In order to compute the second term on the r.h.s. of Eq. (4.13) we need to first find an expression for the Levi-Civita connection coefficients $\Gamma^3_{jk}$. For the metric $h_{ij}$ defined in Eq. (4.10)

$$\begin{aligned}\Gamma^i_{jk} &= \frac{1}{2}h^{il}\left(\partial_j h_{lk}+\partial_k h_{jl}-\partial_l h_{jk}\right)\\ &= \sum_l \frac{1}{2}\frac{1}{f}\delta_{il}\left(\partial_j\left(f\delta_{lk}\right)+\partial_k\left(f\delta_{jl}\right)-\partial_l\left(f\delta_{jk}\right)\right)\\ &= \frac{1}{2}\frac{1}{f}\left(\delta_{ik}\partial_j f+\delta_{ji}\partial_k f-\delta_{jk}\partial_i f\right). \qquad (4.15)\end{aligned}$$

Therefore,

$$\Gamma^3_{jk} = \frac{1}{2f}\left(\delta_{3k}\partial_j f+\delta_{j3}\partial_k f\right), \tag{4.16}$$

or, in a matrix form,

$$\Gamma^3 = \frac{1}{2f}\begin{pmatrix}0 & 0 & f_x\\ 0 & 0 & f_y\\ f_x & f_y & 0\end{pmatrix}. \tag{4.17}$$

Finally, the second term of the flow from Eq. (4.13) becomes

$$\Gamma^3_{jk}\partial_\mu X^j\partial_\nu X^k g^{\mu\nu} = \frac{\nabla f\cdot\nabla u}{f^2\left(1+|\nabla u|^2\right)}. \tag{4.18}$$

Using Eq. (4.14) and Eq. (4.18) we obtain the level set evolution

$$u_t = \frac{1}{f\sqrt{1+|\nabla u|^2}}\mathrm{div}\left(\frac{\nabla u}{\sqrt{1+|\nabla u|^2}}\right)+\frac{\nabla f\cdot\nabla u}{f^2\left(1+|\nabla u|^2\right)}. \tag{4.19}$$

Finally, we use our freedom of parametrization and multiply the above evolution by the pre-factor of $f^2\left(1+|\nabla u|^2\right)$, to obtain

$$u_t = \mathrm{div}\left(f\frac{\nabla u}{\sqrt{1+|\nabla u|^2}}\right)\sqrt{1+|\nabla u|^2}. \tag{4.20}$$

Note, that up to the additional constant 1, this formulation aligns with the level set formulation of the geodesic active contour model given in Eq. (4.3). Since the surface definition in Eq. (4.8) is arbitrary, we can choose the aspect ratio between $du$ and $dx, dy$ to be as large as we want. Thus, the constant 1 can be regarded as an $\varepsilon\to 0$ that vanishes upon the right selection of this aspect ratio. We thereby demonstrated that the geodesic active contour model in its level set

formulation, can also be viewed as a surface that minimizes the Polyakov action with a specific selection of metric tensors for the parametrization and the embedding space. The minimizer is obtained by application of the LBO, yet again in a gradient descent heat flow fashion.

## 5. Conclusions

The Laplace Beltrami operator has been shown to provide a modeling construction approach which is useful for shape and image selective smoothing, for shape matching, and for object segmentation in images. We allowed ourselves to select the relevant metric and the coordinates upon which the operator is acting according to the problem at hand. The freedom of these settings allowed us to link between state of the art solutions for shape and image processing and analysis. We expect these observations and tool design methodology to pave the way for new solutions of novel problems in the domain of imaging sciences.

## 6. Acknowledgements

This work has been supported by grant agreement no. 267414 of the European Community FP7-ERC program.

## References

[1] Yonathan Aflalo and Ron Kimmel. Spectral multidimensional scaling. *Proceedings of the National Academy of Sciences*, 110(45):18052–18057, 2013.

[2] Yonathan. Aflalo, Ron Kimmel, and Dan Raviv. Scale invariant geometry for nonrigid shapes. *SIAM Journal on Imaging Sciences*, 6(3):1579–1597, 2013.

[3] Luis Alvarez, Frédéric Guichard, Pierre-Louis Lions, and Jean-Michel Morel. Axioms and fundamental equations of image processing. *Archive for Rational Mechanics and Analysis*, 123(3):199–257, 1993.

[4] M. Belkin and P. Niyogi. Laplacian eigenmaps for dimensionality reduction and data representation. *Neural Comput.*, 15(6):1373–1396, 2003.

[5] P.J. Besl and N.D. McKay. A method for registration of 3-D shapes. *IEEE Transactions on Pattern Analysis and Machine Intelligence*, 14(2):239–256, 1992.

[6] I. Bogdanova, X. Bresson, J. P. Thiran, and P. Vandergheynst. Scale space analysis and active contours for omnidirectional images. *Image Processing, IEEE Transactions on*, 16(7):1888–1901, 2007.

[7] X. Bresson, P. Vandergheynst, and J. P. Thiran. Multiscale active contours. *Scale Space and PDE Methods in Computer Vision*, pages 167–178, 2005.

[8] A. M. Bronstein, M. M. Bronstein, and R. Kimmel. Generalized multidimensional scaling: A framework for isometry-invariant partial surface matching. *Proceedings of the National Academy of Science*, pages 1168–1172, 2006.

[9] A. M. Bronstein, M. M. Bronstein, R. Kimmel, M. Mahmoudi, and G. Sapiro. A Gromov-Hausdorff framework with diffusion geometry for topologically-robust non-rigid shape matching. *International Journal of Computer Vision*, 89(2-3):266–286, 2010.

[10] A.M. Bruckstein, G. Sapiro, and D. Shaked. *Affine-invariant Evolutions of Planar Polygons*. CIS report: ham-@Merkāz le-Ma?arākôt Nevônôt. 1992.

[11] V. Caselles, R. Kimmel, and G. Sapiro. Geodesic active contours. *International journal of computer vision*, 22(1):61–79, February 1997.

[12] Y. Chen and G. Medioni. Object modeling by registration of multiple range images. In *Proceedings of IEEE International Conference on Robotics and Automation*, volume 3, pages 2724 –2729, 1991.

[13] L. D. Cohen and R. Kimmel. Global minimum for active contour models: A minimal path approach. *International Journal of Computer Vision*, 24(1):57–78, 1997.

[14] R. R. Coifman and S. Lafon. Diffusion maps. *Applied and Computational Harmonic Analysis*, 21(1):5 – 30, 2006. Special Issue: Diffusion Maps and Wavelets.

[15] K. Dabov, A. Foi, V. Katkovnik, and K. Egiazarian. Image denoising by sparse 3-d transform-domain collaborative filtering. *IEEE Transactions on Image Processing*, pages 2080–2095, 2007.

[16] A. Elad (Elbaz) and R. Kimmel. On bending invariant signatures for surfaces. *IEEE Trans. on Pattern Analysis and Machine Intelligence (PAMI)*, 25(10):1285–1295, 2003.

[17] M. Hilaga, Y. Shinagawa, T. Kohmura, and T.L. Kunii. Topology matching for fully automatic similarity estimation of 3D shapes. In *ACM SIGGRAPH 2001*, Los Angeles, CA, 12-17 August 2001.

[18] Z. Karni and C. Gotsman. Spectral compression of mesh geometry. In *Proceedings of the 27th annual conference on Computer graphics and interactive techniques*, SIGGRAPH '00, pages 279–286, New York, NY, USA, 2000. ACM Press/Addison-Wesley Publishing Co.

[19] B. Levy. Laplace-beltrami eigenfunctions towards an algorithm that "understands" geometry. *Conference on Shape Modeling and Applications, 2006. SMI 2006. IEEE International*, pages 13–13, 2006.

[20] F. Mémoli and G. Sapiro. A theoretical and computational framework for isometry invariant recognition of point cloud data. *Foundations of Computational Mathematics*, 5(3):313–347, 2005.

[21] R. Osada, T. Funkhouser, B. Chazelle, and D. Dobkin. Shape distributions. *ACM Transactions on Graphics*, 21(4):807–832, 2002.

[22] S. Osher and J. A. Sethian. Fronts propagating with curvature-dependent speed: algorithms based on Hamilton-Jacobi formulations. *Journal of computational physics*, 79(1):12–49, 1988.

[23] D. Raviv, A. M. Bronstein, M. M. Bronstein, R. Kimmel, and N. Sochen. Affine-invariant geodesic geometry of deformable 3d shapes. *Computers & Graphics*, 35(3):692–697, 2011.

[24] A. Roussos and P. Maragos. Tensor-based image diffusions derived from generalizations of the total variation and Beltrami functionals. In *ICIP*, September 2010.

[25] Leonid I. Rudin, Stanley Osher, and Emad Fatemi. Nonlinear total variation based noise removal algorithms. *Phys. D*, 60(1-4):259–268, November 1992.

[26] N. Sochen, R. Kimmel, and A. M. Bruckstein. Diffusions and confusions in signal and image processing. *Journal of Mathematical Imaging and Vision*, 14(3):195–209, 2001.

[27] N. Sochen, R. Kimmel, and A.M. Bruckstein. Diffusions and confusions in signal and image processing. *Journal of Mathematical Imaging and Vision*, 14(3):195–209, 2001.

[28] N. Sochen, R. Kimmel, and R. Malladi. A general framework for low level vision. *IEEE Trans. on Image Processing*, pages 310–318, 1998.

[29] Nir A. Sochen. Stochastic processes in vision: From langevin to beltrami. *Computer Vision, IEEE International Conference on*, 1:288, 2001.

[30] C. Tomasi and R. Manduchi. Bilateral filtering for gray and color images. In *Proc. IEEE ICCV*, pages 836–846, 1998.

[31] C. Tomasi and R. Manduchi. Bilateral filtering for gray and color images. In *Proceedings of the Sixth International Conference on Computer Vision*, ICCV '98, pages 839–, Washington, DC, USA, 1998. IEEE Computer Society.

[32] A. Wetzler and R. Kimmel. Efficient beltrami flow in patch-space. In *Proceedings of the 3rd International Conference on Scale Space and Variational Methods in Computer Vision 2011*, volume 6667, pages 134–143. Springer, 2011.

GIP Lab, Technion, Haifa 32000, Israel • yaflalo@cs.technion.ac.il • nastyad@cs.technion.ac.il • ron@cs.technion.ac.il • twerd@cs.technion.ac.il